(Received 31 August 2024, Accepted 2 October 2024, Scheduled 12 October 2024)

Array Pattern Synthesis Using a New Adaptive Trapezoid Window Function for Sidelobe Suppression and Nulls Control

Jafar Ramadhan Mohammed*

College of Electronics Engineering, Ninevah University, Mosul 41002, Iraq

ABSTRACT: Conventional sidelobe reduction methods such as analytical or parametric approaches and complex numerical optimization approaches were accomplished via specific tapering windows. Among all of the tapering windows a rectangular window gives the simplest array feeding network, narrower beamwidth, and highest directivity. The only drawback is its highest sidelobe level due to sharp edges at the array ends. In this paper, a simple trapezoid taper window which is something between typical rectangular and triangular windows is first suggested as the best compromise between uniform and nonuniform amplitude window functions. Then, it is further developed by making it adaptive or adjustable by including a number of controllable-amplitude elements in the linear edges of the trapezoid window. Thus, the proposed taper window becomes very flexible to accommodate different user-defined constraints. To find the optimal values of those controllable-amplitude elements, a genetic optimization algorithm is used to design and optimize the trapezoid window such that the desired sidelobe peaks and controlled nulls can be met while maximizing the complexity reduction as much as possible. The linear and planar antenna arrays are simulated to validate the superiority of the proposed taper window.

1. INTRODUCTION

A phased antenna array with electronically scanned capability can create a major beam of radio wave and steer it to a point in any direction without moving the antenna system [1]. Many applications such as tracking radar, wireless communications, and remote sensing use two-dimensional planar phased arrays with symmetrical patterns to control the direction of the major beam toward the desired direction and reduce the sidelobes or place nulls toward interfering directions [2, 3].

In general, the far-field antenna pattern can be obtained by taking the Fourier transform of the antenna's aperture illumination function [4]. Consequently, tapering the amplitude and/or the phase of the array's aperture illumination can reduce the undesirable sidelobes and shape the array's far-field pattern [5]. Accordingly, many tapering functions have been proposed in the literature [6, 7], and they become common for antenna array pattern synthesis of all types. Among all of these tapering functions, only rectangular (or uniform) window gives narrower beamwidth and the highest directivity. The main drawback of this taper function is its highest sidelobe level due to sharp edges or amplitude discontinuities at the ends of the taper. Thus, many other tapering functions have been designed to have a nonuniform envelope with the highest amplitudes at the array's centre and gradually decreased values toward the aperture's ends according to the designed taper function. In fact, every element of the array is individually assigned a specific taper's value which practically needs a very high tunable attenuator to realize it. For large arrays, the resulting taper's hardware becomes costly and complex. Moreover, imparting a nonuniform amplitude taper to an array aperture can be problematic where the beamwidth of its array pattern can be significantly widened, thus reducing the array's directivity [8].

Apart from the deterministic or parametric window functions, global optimization algorithms such as genetic algorithm [9], particle swarm optimization [10], convex optimization [11], and many other algorithms have also been used to optimize the amplitude and/or phase of the tapered elements to get the optimum performance and minimized sidelobes.

The tapering functions have been implemented at the subarray level instead of its elemental radiators [12–14]. Controlling the signal's amplitude and phase at the subarray output reduces the number of needed hardware components, but it may cause distortion in the subarray's far-field pattern [15, 16].

Partially tapering functions either by controlling a few existing side elements [17–19] or by adding extra side elements [20, 21] have also been suggested for specific sidelobe suppression or nulls control. It is proved that partially tapering functions are more preferable than those conventional fully tapering functions especially when the number of interfering signals is much smaller than the total number of the array elements.

In this paper, a new trapezoid taper window, which is something between typical rectangular and triangular windows is first introduced. Its performance in trading-off between desired sidelobe peaks and main beamwidths is highlighted with comparison to many other existing taper windows. Then, it is further developed by including a number of controllable-amplitude elements in the linear edges of the trapezoid window. Thus, it becomes adaptive and flexible to accommodate different designer's requirements or user-defined constraints.

* Corresponding author: Jafar Ramadhan Mohammed (jafar.mohammed@uoninevah.edu.iq).

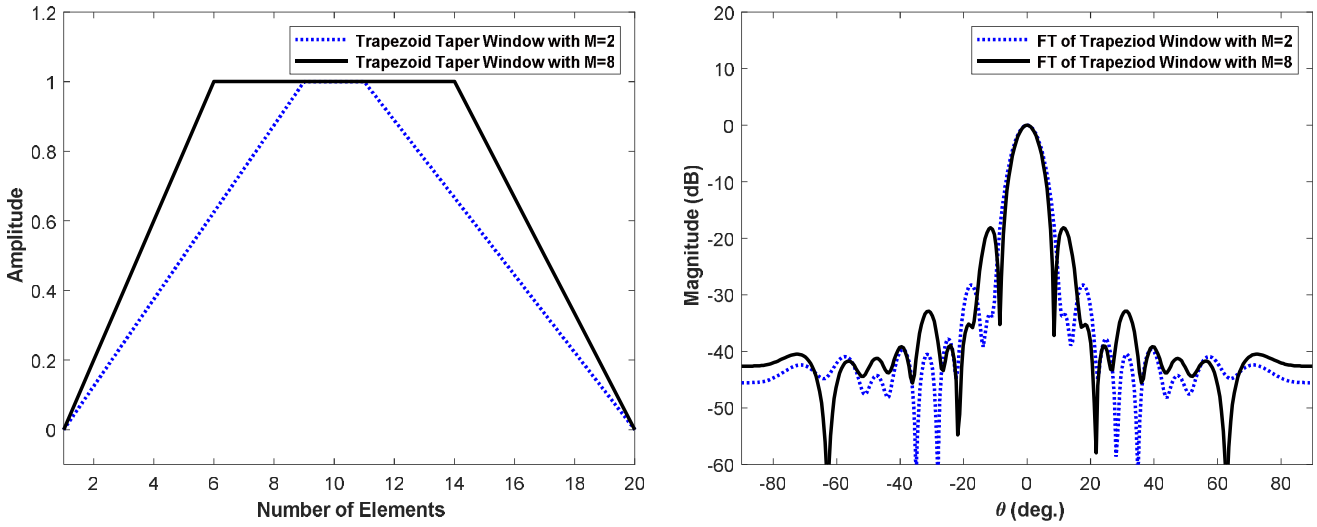

FIGURE 1. Trapezoid taper windows and their corresponding FT patterns.

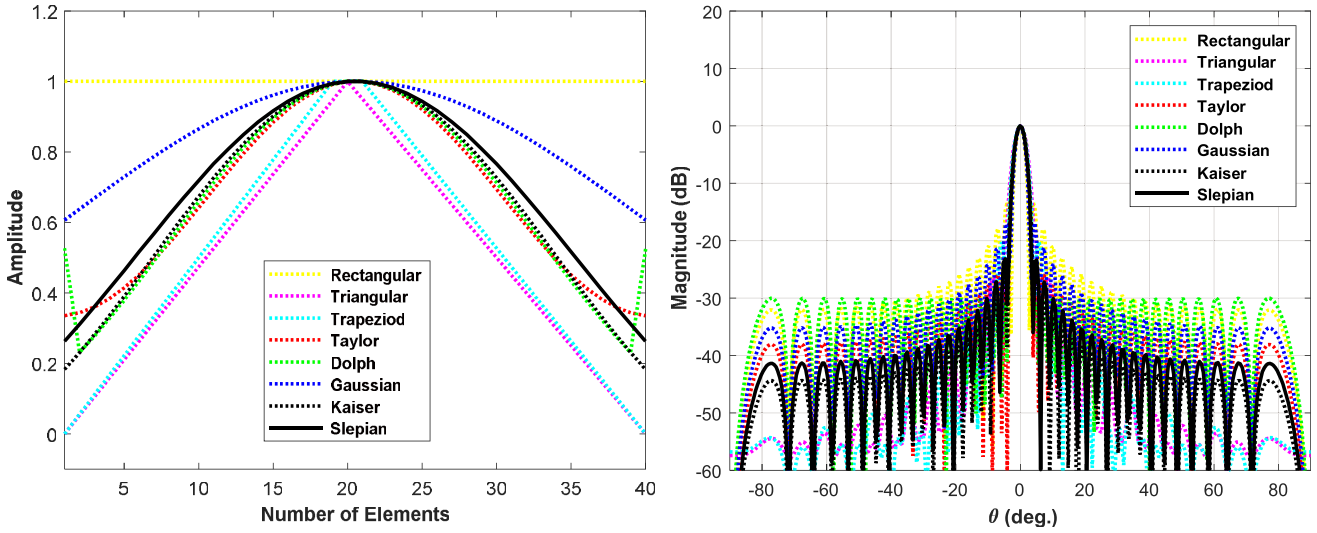

FIGURE 2. Comparison between various taper windows and their corresponding FT pattern.

An optimization based on a genetic algorithm is used to optimize these controllable elements in the linear parts on both sides of the array's aperture. The number and location of the controllable elements and their amplitudes are optimized to obtain desired sidelobe peaks and steered nulls in the linear and planar antenna arrays. Since the resulting adaptive trapezoid taper function has a number of unity-amplitudes at the flat-top center and nonsharp linear edges, it will give a best compromise between the main beamwidths and sidelobe peaks. Moreover, the remaining array elements at the flat-top center of the resulting adaptive trapezoid taper have unity or fixed amplitudes, thus, it enjoys a relatively simple feeding network.

2. THE TRAPEZOID TAPER WINDOW

Consider an amplitude taper function given by w_n where $n = 1, 2, ..., N$ is the array elements index. For simplicity, it is assumed that the total number of array elements N is even, and the inter-element spacing d is uniform which is equal to $\frac{\lambda}{2}$. A deterministic taper function might be any one of the conventional common window functions such as Hamming, Taylor, Dolph, or any other type [6]. The Fourier transform of such amplitude tapers with equally-spaced elements will yield a far-field array pattern given by

$$FF_o(\theta) = \sum_{n=1}^{N/2} w_n \cos\left[\frac{(2n-1)}{2} kd \sin\theta\right] \qquad (1)$$

where $k = \frac{2\pi}{\lambda}$, λ is the wave length, and θ is the direction of arrival angle from the broadside. The array aperture length is $L = d \times N$. Let $w_n = a_n e^{P_n}$ where a_n and P_n represent the amplitude and phase of the tapered window w_n. In this work, we consider amplitude-only control (i.e., varying a_n and zero phases $p_n = 0$). a_n will be calculated using trapezoid taper which is something between common rectangular and triangular windows. It has a flat center section and linear tapers

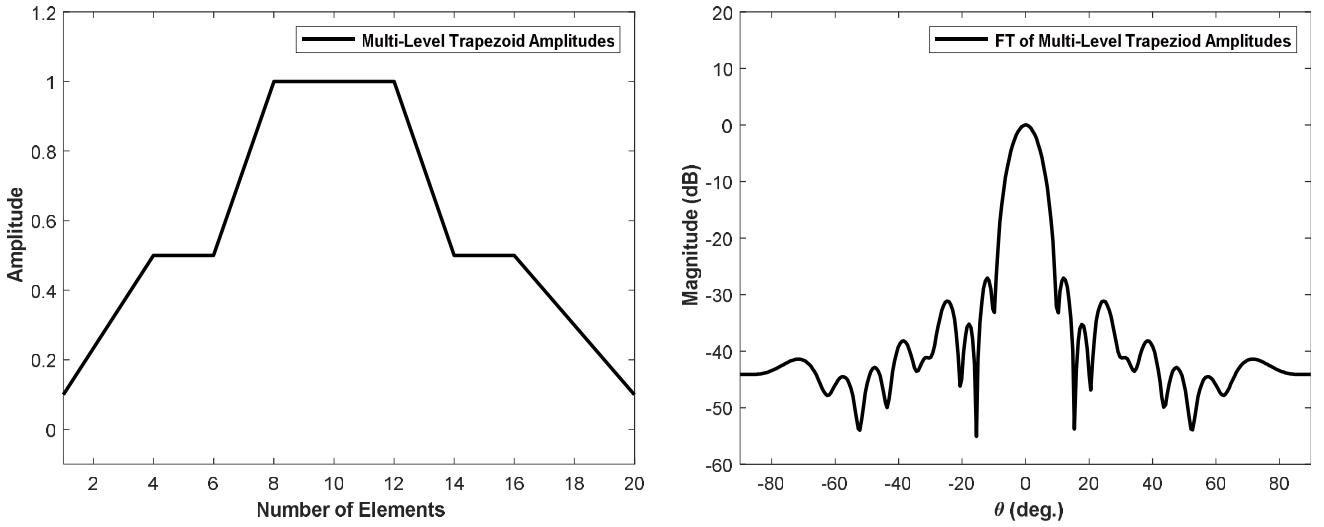

FIGURE 3. Multi-level trapezoid amplitudes and it's corresponding FT pattern.

toward the edges. Like the other typical tapers, this taper is deterministic (or parametric) window where its amplitudes can be calculated by

$$a_n = \begin{cases} \frac{2}{1+2M} & n \leq M \\ \frac{2(1-2n)}{1-(2M)^2} & M < n \leq N \\ 0 & n \geq N \end{cases} \quad (2)$$

where M is the number of the flat-top central elements of the trapezoid window, which have unit-amplitudes. Note that the trapezoid window can also be generated as the difference between two triangle windows. The far-field array pattern can be obtained by taking the Fourier transform (FT) of (2). Fig. 1 shows the trapezoid window as well as its corresponding FT for two cases $M = 2$, $M = 8$ and for a total array elements equal to $N = 20$. It can be seen that its sidelobe level (SLL) and half power beamwidth (HPBW) for $M = 2$ case are 28.6 dB and 7.6°, respectively, and for $M = 8$ case, they change to -18.3 dB and 7.0°, respectively. A comparison of such a trapezoid window with other typical windows is shown in Fig. 2. Clearly, the trapezoid window gives a good compromise between SLL and HPBW compared to other windows. The proposed trapezoid window is further modified to include multi-level amplitudes for seeking a greater reduction in the array feeding complexity. The modified trapezoid window with multi-level amplitudes and its corresponding array pattern are shown in Fig. 3.

3. THE TRAPEZOID WINDOW WITH CONTROLLED AMPLITUDE-TAPERS

In the previous two variants of the proposed trapezoid window, the linear parts (i.e., the non-unity amplitudes of the trapezoid taper) at the sides of the array are non-optimal due to its simple parametrical calculation. Better performance can be obtained by further developing this window by including a number of the controllable-amplitude elements in the linear regions of the original trapezoid window. A genetic algorithm can be used to optimize the amplitudes of these controllable side elements. The optimization variables are: the number of the optimized side-elements at each side of the array and their amplitudes, the number of the fixed elements in the flat-top center region of this window, and the number of the fixed elements in the flat-middle region.

To proceed with the optimized multi-level trapezoid taper, the array elements of a linear antenna array are first divided into three different subsets according to their locations in the trapezoid regions. These regions or sections are: the flat-top central region which is assumed to have a total of M_1 elements, two outer linear regions which are assumed to have a total of M_2 elements, and the middle fixed-element region consists of M_3 elements. Thus, the total number of array elements is $N = M_1 + M_2 + M_3$, and their amplitudes are $a_n = a_{m_1} + a_{m_2} + a_{m_3}$. As in the original trapezoid window, the first subset M_1 elements have unit-amplitudes, thus, they

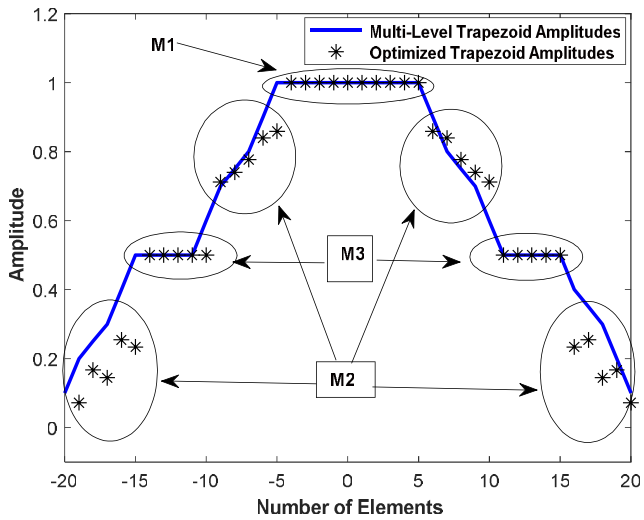

FIGURE 4. Three subsets M_1, M_2, and M_3 of the trapezoid amplitudes for $N = 40$, $M_1 = M_3 = 10$, and $M_2 = 20$.

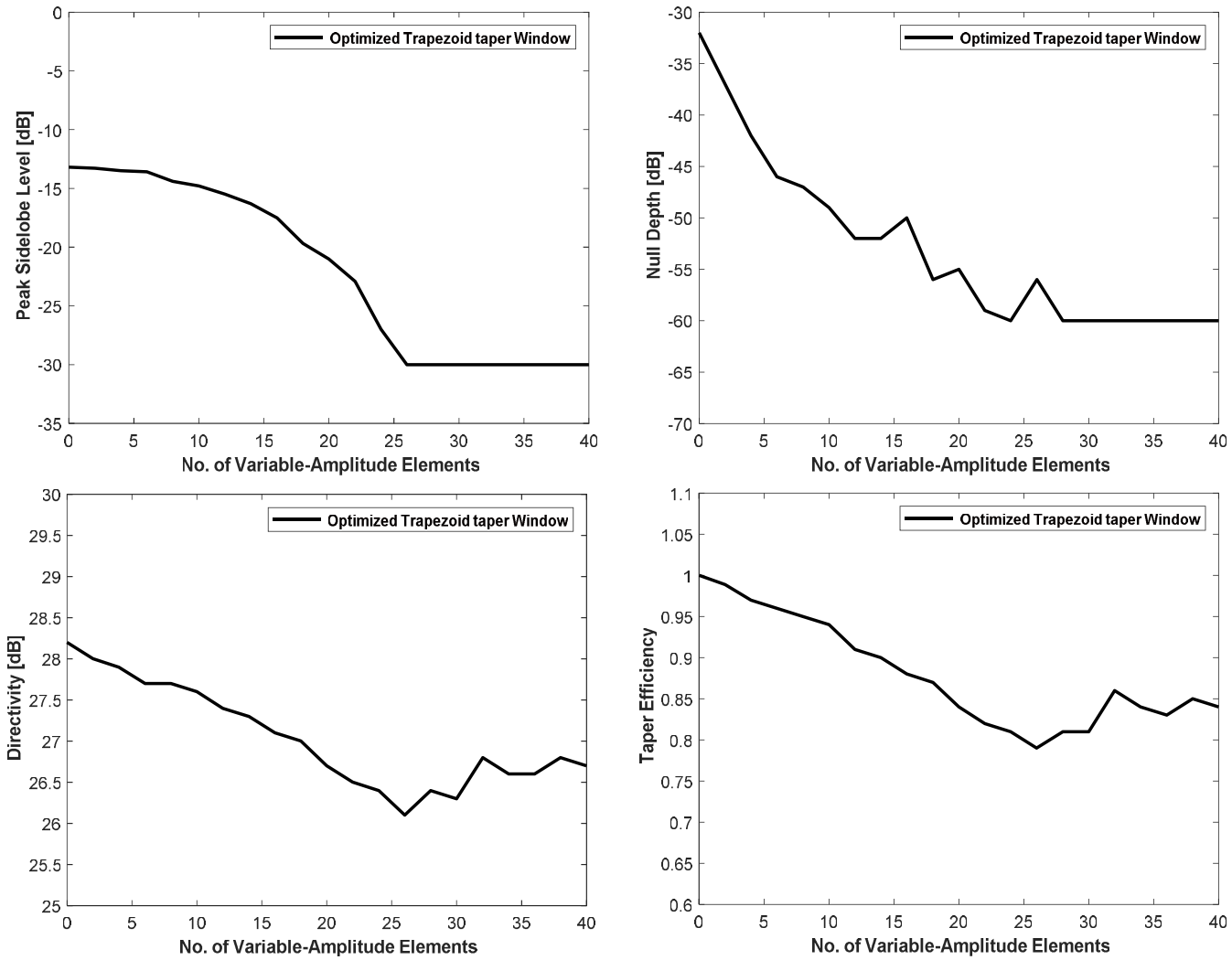

FIGURE 5. Variation of PSLL, ND, D, and TE of the optimized trapezoid window versus the number of variable-amplitude elements M_2.

are fixed, $a_{m_1} = 1$ for $m_1 = 1, 2, ..., M_1$. The second subset M_2 elements have variable amplitudes, thus, they are controllable which can be computed either parametrically according to (2) or optimally by means of an optimization method. The third subset M_3 elements have half amplitudes $a_{m_3} = 0.5$ for $m_3 = 1, 2, ..., M_3$ to produce multi-level taper as shown in Fig. 4. Note that due to the existence of subset M_3, the elements of M_2 may be divided into two parts in each side of the array.

Since the amplitude tapers of the M_2 will be optimized, its new amplitudes can be written as

$$a_{M_2} = a_{m_2} + \Delta_{m_2} \quad m_2 = 1, 2, ..., M_2 \tag{3}$$

where Δ_{m_2} is the amount of amplitude changes with respect to the original linear trapezoid amplitudes a_{m_2}. Then, the far-field array pattern of these corresponding three amplitude tapers can be written as

$$FF(\theta) = \underbrace{\sum_{m_1=1}^{M_1} a_{m_1} \cos\left[\frac{(2m_1-1)}{2} kd\sin\theta\right]}_{\text{Flat-Top Central Subset}} + \underbrace{\sum_{m_2=1}^{M_2} a_{m_2} \cos\left[\frac{(2m_2-1)}{2} kd\sin\theta\right]}_{\text{Outer Variable Subset}} + \underbrace{\sum_{m_3=1}^{M_3} a_{m_3} \cos\left[\frac{(2m_3-1)}{2} kd\sin\theta\right]}_{\text{Middle Fixed Subset}} \tag{4}$$

As mentioned, the normalized amplitudes of $a_{m_1} = 1$ for M_1 elements, $a_{M_2} = a_{m_2} + \Delta_{m_2}$ for M_2 elements, and $a_{m_3} = 0.5$ for M_3 elements. Thus, (4) can be rewritten in a simplified form as

$$FF(\theta) = \sum_{n=1}^{N/2} a_n \cos\left[\frac{(2n-1)}{2} kd\sin\theta\right] + \sum_{m_2=1}^{M_2} \Delta_{m_2} \cos\left[\frac{(2m_2-1)}{2} kd\sin\theta\right] \tag{5}$$

From (5) it is clear that there are only M_2 variables to be optimized instead of N total array variables for a prespecified SLL, HPBW, and nulls control. To maintain the array pattern of (5)

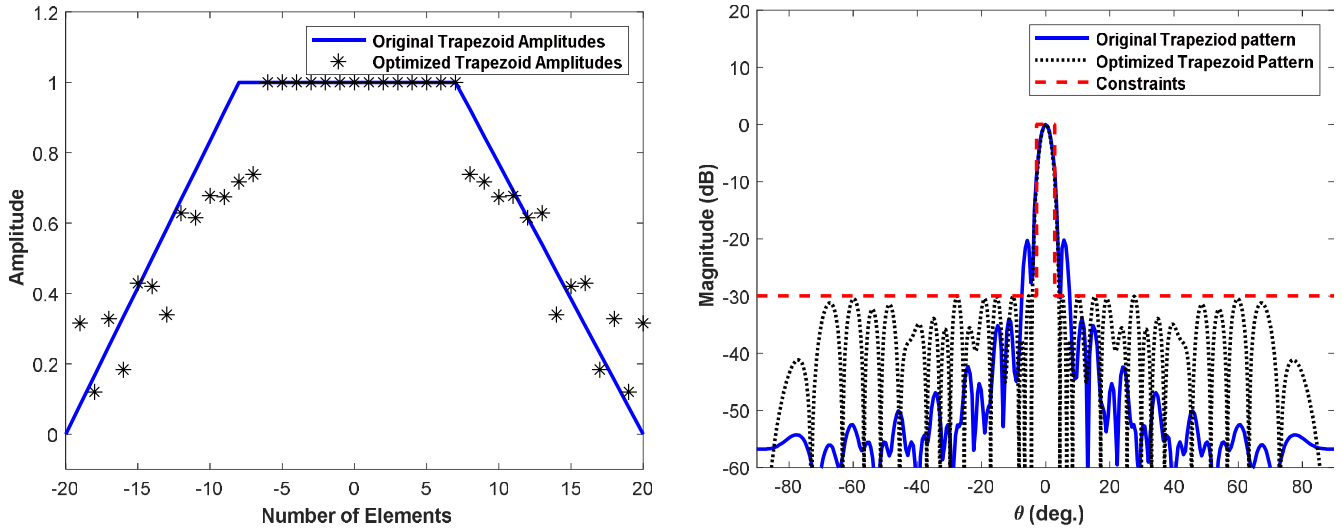

FIGURE 6. Original and optimized trapezoid tapers and their corresponding patterns for $N = 40$, $M_1 = 14$, $M_2 = 26$, and $M_3 = 0$.

within the user-defined constraint (UDC) limits, the difference between them, $E(\theta)$, should be minimized as follows

$$E(\theta_s) = \sum_{s=1}^{S} |FF(\theta_s) - \text{UDC}(\theta_s)|^2 \tag{6}$$

where $s = 1, 2, ..., S$ are the sample points between these two patterns, and the UDC is given by

$$\text{UDC}(\theta) = \begin{cases} 20\log_{10}(\text{SLL}_{\text{limit}}), & 90^\circ \le |\theta| \le \text{FNBW} \\ 20\log_{10}\frac{FF(\theta)}{\max(FF(\theta))}, & \text{FNBW} \le \theta \le \text{FNBW} \end{cases} \tag{7}$$

4. SIMULATION RESULTS

This section carries out various simulations to demonstrate the validity of the proposed trapezoid taper and its developed variants in reducing the SLL, placing multiple wide and deep nulls in the array pattern using a partial amplitude control.

In all examples, a symmetrical uniform linear array with $N = 40$ elements and equal inter-element spacing $d = \frac{\lambda}{2}$ was examined. The specification parameters of the used genetic optimization algorithm were: the number of iterations was 1000; the number of population was set to 50; the number of marriages was 25; the number of crossovers was 2; a uniform crossover was chosen, and the selection was tournament. The mutation probability was set to 0.04, and the eligible tournament was set to 10.

In the first example, the performance metrics in terms of peak sidelobe level (PSLL), null depth (ND), directivity (D), and the taper efficiency (TE) of the optimized trapezoid window under different numbers of variable-amplitude elements, M_2, and zero half-amplitude elements, $M_3 = 0$ have been numerically studied. Fig. 5 illustrates such results. It can be seen from these results that the PSLL and ND are both improved with increased number of variable-amplitude elements, M_2. In other words they are both getting worse with increased number of unit-amplitude elements, M_1, until they reach the typical rectangular window values at $M_1 = 40$ and $M_2 = 0$. The D and TE values are both getting lower with increasing the number of variable-amplitude elements, M_2. They are both at their highest values only when $M_1 = 40$ and $M_2 = 0$ which corresponds to the typical rectangular taper window.

In the second example, the array patterns of the original non-adaptive trapezoid and the optimized adaptive trapezoid windows for $M_1 = 14$, $M_2 = 26$, $M_3 = 0$ elements on both sides of the array center are illustrated. The user-defined constraints in this scenario were set according to the dashed red-line limits where the peak sidelobe level is assumed to not exceed $\text{SLL}_{\text{limit}} = -30$ dB. The initial pattern of the original non-adaptive trapezoid window was also included in this figure for comparison purpose. Fig. 6 shows these array patterns and their corresponding taper windows. The PSLL in the original and optimized trapezoid patterns were -20 dB and -30 dB, respectively. The superiority of the optimized adaptive trapezoid window compared to its original non-adaptive counterpart is clear.

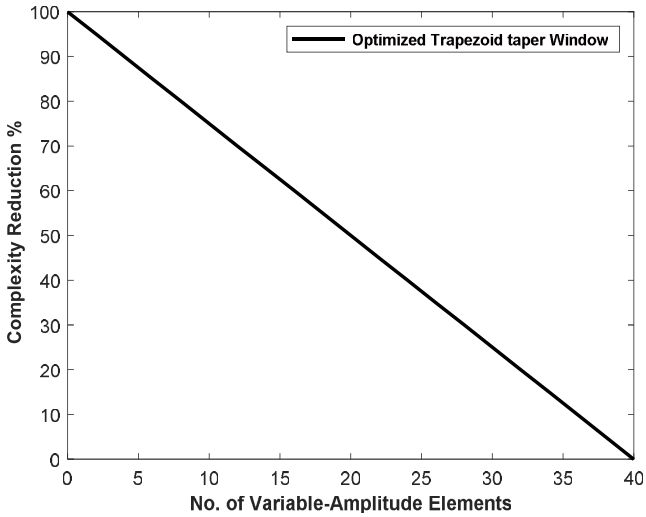

FIGURE 7. Variation of CR% of the optimized trapezoid window versus the number of variable-amplitude elements M_2.

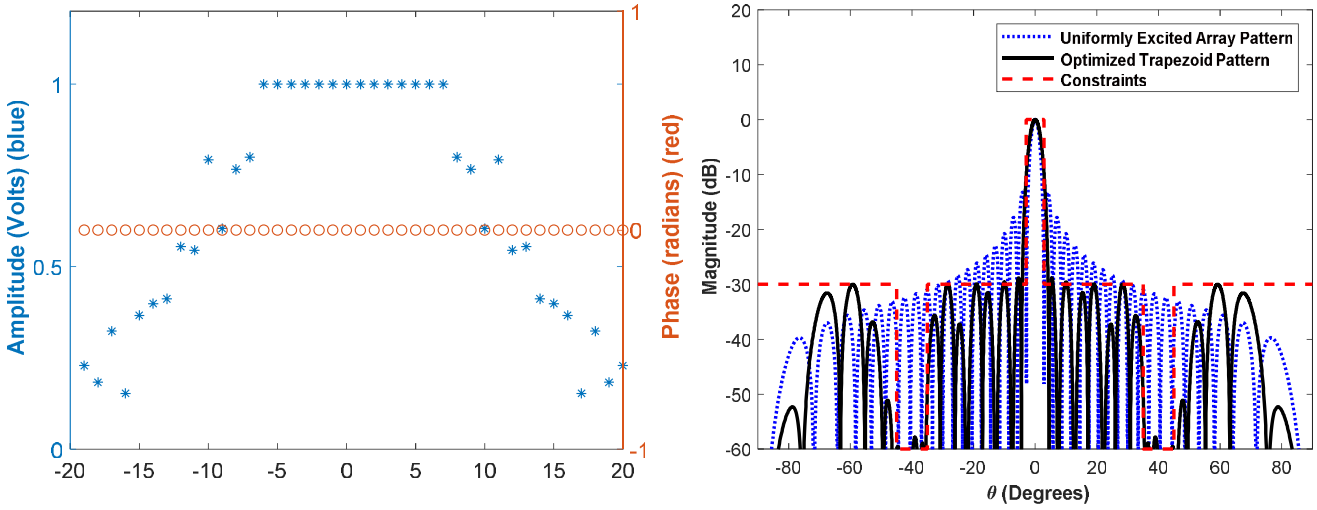

FIGURE 8. Optimized trapezoid taper and its corresponding pattern for $N = 40$, $M_1 = 14$, $M_2 = 26$, and $M_3 = 0$.

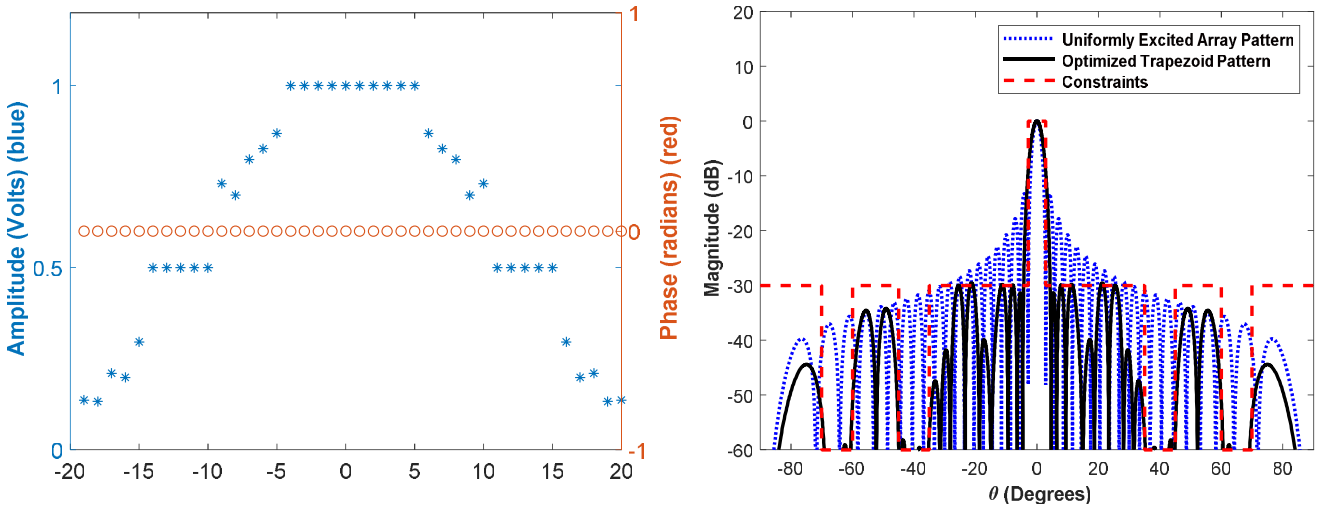

FIGURE 9. Optimized trapezoid taper and its corresponding pattern for $N = 40$, $M_1 = 10$, $M_2 = 20$, and $M_3 = 10$.

In the third example, the array complexity in terms of the number of variable amplitude elements, M_2, in the outer sections of the trapezoid window is studied. The following metric is used for calculating the complexity reduction (CR)

$$\text{CR} = \left[\frac{\begin{array}{c}\text{Total number of array elements} \\ -\text{Total number of variable elements}\end{array}}{\text{Total number of array elements}} \right] \times 100\% \quad (8)$$

This equation is applied to the optimized trapezoid window under various numbers of M_1, M_2, and $M_3 = 0$. The CR% result is shown in Fig. 7. It can be seen that the complexity reduction of the feeding network is linearly proportional to the number of adaptive-amplitude elements, M_2. For $M_2 = 20$ variable elements, the CR% is 50%. The CR% of the common typical Dolph taper window is CR% $= 100\%$ where all of its amplitude elements are variable, and none of them are fixed. This validates the simplicity of the proposed trapezoid window compared to other nonuniform windows.

In the next example, the array pattern and its corresponding optimized adaptive trapezoid window for $M_1 = 14$, $M_2 = 26$, and $M_3 = 0$ are illustrated in Fig. 8 where CR $= 35\%$. Besides such reduction in the complexity, the PSLL was maintained below -30 dB, and two wide-deep nulls around the centers at $\theta = \pm 40^\circ$ (from $\theta = \pm 35^\circ$ up to $\theta = \pm 45^\circ$ with width of each of them equal to 10°, and the required depth is set to -60 dB, respectively) are also validated. In another example, the array pattern and its corresponding optimized adaptive trapezoid window for $M_1 = 10$, $M_2 = 20$, and $M_3 = 10$ are illustrated in Fig. 9 where CR $= 50\%$. Besides such a great reduction in the complexity, the PSLL was maintained below -30 dB, and four wide-deep nulls around the centers at $\theta = \pm 40^\circ$ and $\theta = \pm 65^\circ$ with depths more than -60 dB were also validated.

Finally, the proposed taper window that has been applied to the one-dimensional linear array is extended to the two-dimensional planar array with a total number of equal-spaced elements equal to 40×40. In this example, two scenarios are considered. The first scenario is the original non-adaptive

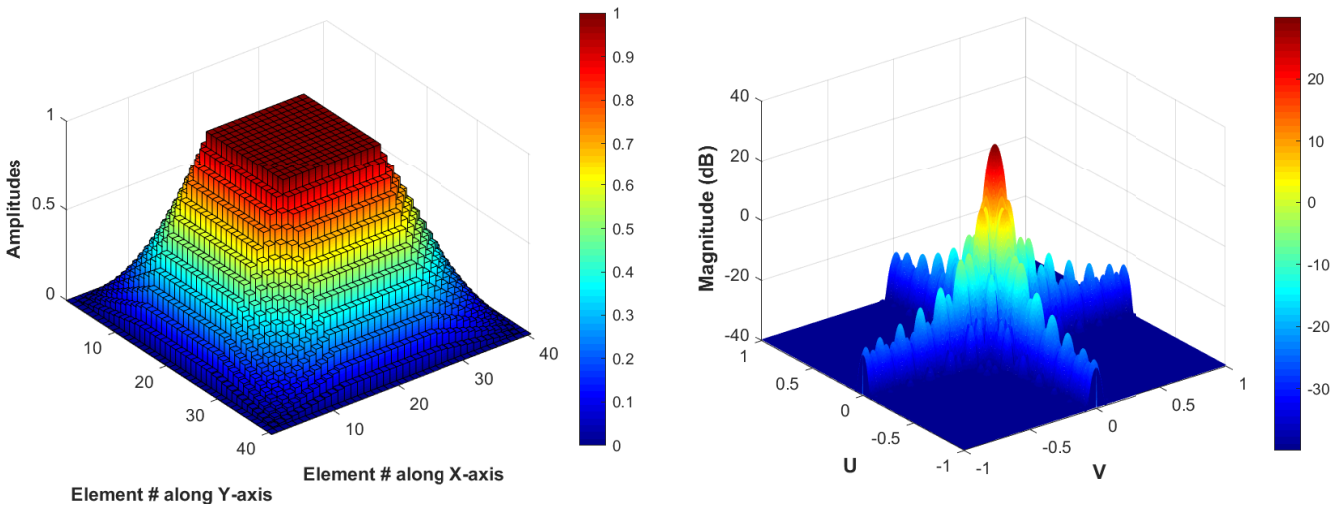

FIGURE 10. Original trapezoid taper and its corresponding pattern for $N = 40 \times 40$, $M_1 = 14 \times 14$, $M_2 = 26 \times 26$, and $M_3 = 0$.

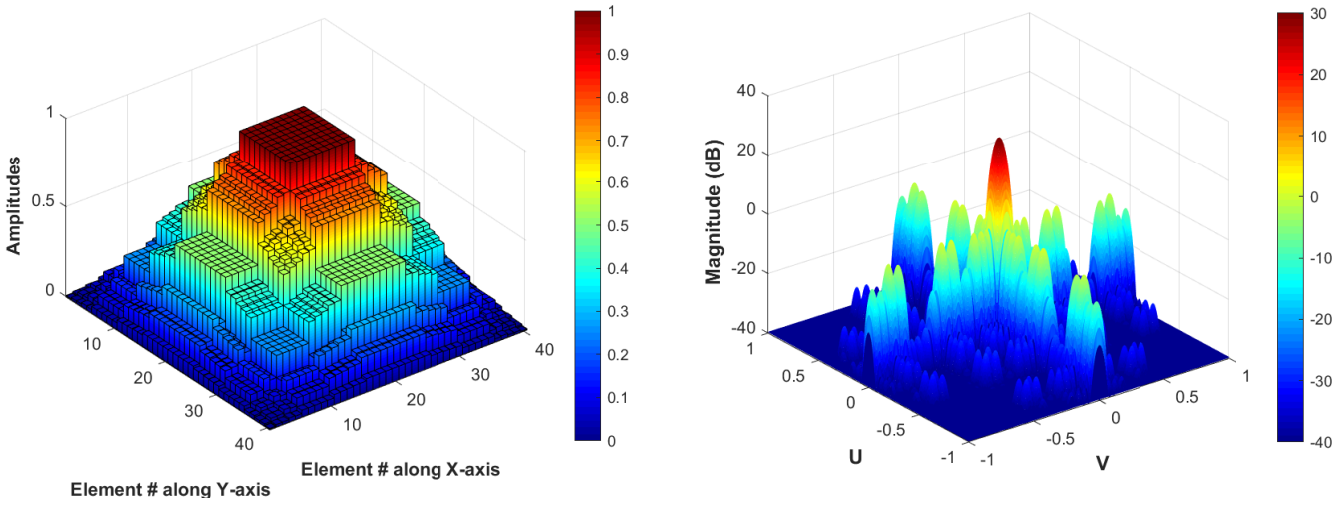

FIGURE 11. Optimized two-dimensional trapezoid taper and its corresponding pattern for $N = 40 \times 40$, $M_1 = 10 \times 10$, $M_2 = 20 \times 20$, and $M_3 = 10 \times 10$.

trapezoid window (see Fig. 10), while the second scenario is the optimized adaptive trapezoid window with $M_1 = 10$, $M_2 = 20$, and $M_3 = 10$ and four wide-deep nulls around the centers $\theta = \pm 40^\circ$ and $\theta = \pm 65^\circ$ (see Fig. 11).

5. CONCLUSIONS

The proposed adaptive trapezoid taper window with controllable-amplitude elements at the taper's edges has been found to best compromise between the sidelobe peaks and main beam widths of the array's pattern. It has a maximum or unit-amplitudes in the center of the window and taper away from the center. Both the unit-amplitude and taper-amplitude parts were made controllable to provide the best performance while optimizing them. By changing the number of the unit-amplitude elements or taper-amplitude elements, the resulting window becomes something between common rectangular and triangular windows. It is worthy to mention that such an adaptive or adjustable taper window is only introduced here for the first time to the best of authors' knowledge, and it is clearly more preferable than all the other existing non-adjustable taper windows. Results show that the proposed adaptive trapezoid taper window can achieve a considerably lower peak sidelobe level to less than -30 dB with a narrower main beamwidth and a less number of the variable-amplitude elements than the results in the literature, which demonstrates its feeding network simplicity.

REFERENCES

[1] Balanis, C. A., *Antenna Theory: Analysis and Design*, 3rd ed., John Wiley & Sons, Hoboken, 2016.

[2] Mohammed, J. R., "Simplified rectangular planar array with circular boundary for side lobe suppression," *Progress In Electromagnetics Research M*, Vol. 97, 57–68, 2020.

[3] Abdulqader, A. J., J. R. Mohammed, and R. H. Thaher, "Antenna pattern optimization via clustered arrays," *Progress In Electromagnetics Research M*, Vol. 95, 177–187, 2020.

[4] Keizer, W. P. M. N., "Fast low-sidelobe synthesis for large planar array antennas utilizing successive fast Fourier transforms of the array factor," *IEEE Transactions on Antennas and Propagation*, Vol. 55, No. 3, 715–722, 2007.

[5] Mohammed, J. R., "A method for thinning useless elements in the planar antenna arrays," *Progress In Electromagnetics Research Letters*, Vol. 97, 105–113, 2021.

[6] Harris, F. J., "On the use of windows for harmonic analysis with the discrete Fourier transform," *Proceedings of the IEEE*, Vol. 66, No. 1, 51–83, 1978.

[7] Oppenheim, A. V., R. W. Schafer, and J. R. Buck, *Discrete-time Signal Processing*, 2nd ed., 465–478, Prentice Hall, Upper Saddle River, N.J., 1999.

[8] Mohammed, J. R. and K. H. Sayidmarie, "Synthesizing asymmetric side lobe pattern with steered nulling in nonuniformly excited linear arrays by controlling edge elements," *International Journal of Antennas and Propagation*, Vol. 2017, No. 1, 9293031, 2017.

[9] Mohammed, J. R., "An optimum side-lobe reduction method with weight perturbation," *Journal of Computational Electronics*, Vol. 18, No. 2, 705–711, 2019.

[10] Jin, N. and Y. Rahmat-Samii, "Advances in particle swarm optimization for antenna designs: Real-number, binary, single-objective and multiobjective implementations," *IEEE Transactions on Antennas and Propagation*, Vol. 55, No. 3, 556–567, 2007.

[11] Shaker, R. R. and J. R. Mohammed, "Obtaining feasible minimum side lobe level for narrow beam width using convex optimization in linear, planar, and random antenna arrays," *The Applied Computational Electromagnetics Society Journal (ACES)*, Vol. 37, No. 7, 811–816, 2022.

[12] Abdulqader, A. J., J. R. Mohammed, and Y. A. Ali, "A T-shaped polyomino subarray design method for controlling sidelobe level," *Progress In Electromagnetics Research C*, Vol. 126, 243–251, 2022.

[13] Haupt, R., "Null synthesis with phase and amplitude controls at the subarray outputs," *IEEE Transactions on Antennas and Propagation*, Vol. 33, No. 5, 505–509, 1985.

[14] Mohammed, J. R., "Synthesizing non-uniformly excited antenna arrays using tiled subarray blocks," *Journal of Telecommunications and Information Technology*, Vol. 4, 25–29, 2023.

[15] Mohammed, J. R., A. J. Abdulqader, and R. H. Thaher, "Array pattern recovery under amplitude excitation errors using clustered elements," *Progress In Electromagnetics Research M*, Vol. 98, 183–192, 2020.

[16] Mohammed, J. R., "Minimizing grating lobes in large arrays using clustered amplitude tapers," *Progress In Electromagnetics Research C*, Vol. 120, 93–103, 2022.

[17] Abdulqader, A. J., J. R. Mohammed, and R. H. Thaher, "Phase-only nulling with limited number of controllable elements," *Progress In Electromagnetics Research C*, Vol. 99, 167–178, 2020.

[18] Mohammed, J. R., "Optimal null steering method in uniformly excited equally spaced linear arrays by optimising two edge elements," *Electronics Letters*, Vol. 53, No. 13, 835–837, Jun. 2017.

[19] Mohammed, J. R., "Element selection for optimized multiwide nulls in almost uniformly excited arrays," *IEEE Antennas and Wireless Propagation Letters*, Vol. 17, No. 4, 629–632, Apr. 2018.

[20] Mohammed, J. R., "A new technique for obtaining wide-angular nulling in the sum and difference patterns of monopulse antenna," *IEEE Antennas and Wireless Propagation Letters*, Vol. 11, 1245–1248, 2012.

[21] Mohammed, J. R. and K. H. Sayidmarie, "Performance evaluation of the adaptive sidelobe canceller system with various auxiliary configurations," *AEU — International Journal of Electronics and Communications*, Vol. 80, 179–185, 2017.